START PAGE

Chapter 12

SWITCHED RELUCTANCE MOTOR (SRM) DRIVES

12.1. INTRODUCTION

SRMs are doubly salient, singly excited electric motors with passive (windingless) rotors. Their concentrated coil phases are turned-on sequentially, to produce torque, through DC voltage pulses which result in unipolar controlled current.

Due to their simple and rugged topology, SRMs have been given considerable attention in the last two decades in the hope of producing alternative low grade and high grade brushless motor electric drives at a lower cost and equivalent performance when compared with AC (induction or synchronous) motor drives.

At the time of this writing the SRM drive enjoys only an incipient market but an aggressive penetration of worldwide markets is expected in the near future. Power ratings of SRMs range from a few watts to practically MW units for low speed control range low dynamics, as well as high grade (servo) applications, especially in thermally and chemically harsh environments.

Given the topological peculiarities of the SRM, a few details are considered in order. Also, the operation of SRM with an active phase only at a time, in the presence of magnetic saturation, with open-loop (voltage PWM) or closed-loop (current control) PWM, requires elaborate digital simulation methods.

The basic strategies for low grade and high grade speed and position control with and without motion sensors are also treated in some detail. Some numerical examples are provided to facilitate quick access to magnitudes for a realistic assessment of performance.

12.2. CONSTRUCTION AND FUNCTIONAL ASPECTS

SRMs are made of laminated stator and rotor cores with $N_s = 2mq$ poles on the stator and N_r poles on the rotor. The number of phases is m and each phase is made of concentrated coils placed on 2q stator poles.

Most favored configurations — amongst many more options — are the 6/4 three-phase and the 8/6 four-phase SRMs (Figure 12.1a, b).

These two configurations correspond to q = 1 (one pair of stator poles (and coils) per phase) but q may be equal to 2, 3 when, for the three-phase machine, we obtain 12/8 or 18/12 topologies applied either for low speed high torque direct drives or for high speed stator-generator systems for

aircraft [2]. The stator and rotor pole angles β_s and β_r are, in general, almost equal to each other to avoid zero torque zones.

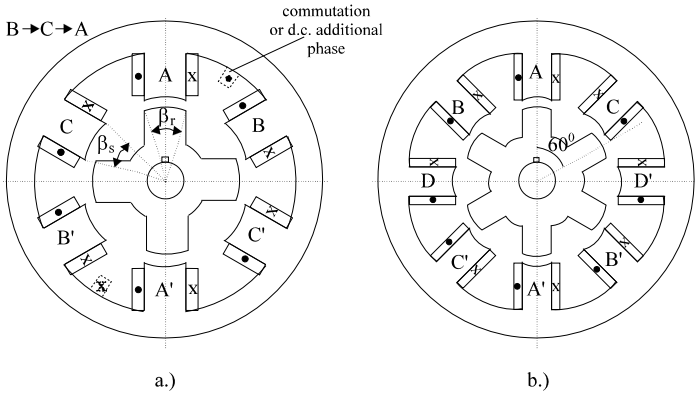

Figure 12.1. Representative SRM configurations

The symmetry of the magnetic circuit leads to the almost zero mutual flux linkage in the SRM phases even under saturated conditions. This means that the SRM may work with m–1 phases since no induced voltage or current will appear in the short-circuited phase. Hence the SRM is more fault tolerant than any AC motor where the interaction between phases is at the core of their principle of operation. The self-inductance of each phase alone thus plays the key role in torque production.

In the absence of magnetic saturation, the phase self-inductance varies linearly with rotor position, while, in presence of saturation, the respective dependence is nonlinear (Figure 12.2).

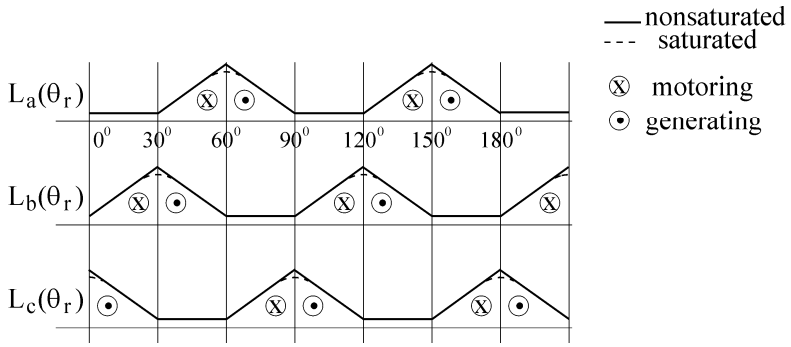

Figure 12.2. The phase inductances and the operation modes of three-phase 6/4 SRM

If the phase flux linkage λ is calculated and plotted versus current for various rotor positions, the $\lambda(\theta_r,i)$ curve family is obtained (Figure 12.3).

The influence of magnetic saturation is evident from Figure 12.3 and is a practical reality in well-designed SRMs, as will be shown later in this section.

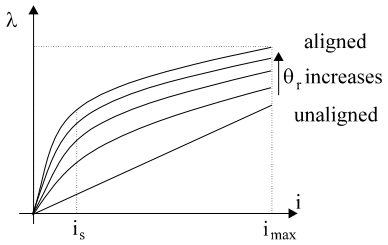

Figure 12.3. Flux / current / position curve family

The instantaneous torque $T_e(i)$ per phase may be obtained through the known coenergy, $W_{mc}(\theta_r)$, formula

$$T_e(i) = \left(\frac{\partial W_{mc}(\theta_r)}{\partial \theta_r}\right)_{i=cons.} \quad ; \quad W_{mc} = \int_0^i \lambda(\theta_r, i)di \tag{12.1}$$

Equation (12.1) demonstrates the necessity of knowing, through calculations or test, the family of curves $\lambda(\theta_r,i)$.

The total instantaneous torque is

$$T_e = \sum_{i=1}^{m} T_e(i) \tag{12.2}$$

Only in the absence of saturation, the instantaneous torque is

$$T_e = \sum_{i=1}^{m} \frac{1}{2} i_i^{\,2} \frac{\partial \lambda_i(\theta_r)}{\partial \theta_r} \tag{12.3}$$

Ideally, a phase is turned-on when rotor poles, along the direction of motion, lay between neighboring stator poles $\theta_{on} = 0$ (Figure 12.4), for the motoring operation mode of the respective phase. Only one voltage pulse is applied for a conduction (dwell) angle $\theta_w = \theta_c - \theta_{on}$ in Figure 12.4. During this period, neglecting the resistive voltage drop, the maximum phase flux linkage λ_{max}, for constant speed ω_r, is

$$\lambda_{max} = \int_0^t V_d dt = V_d \frac{\theta_w}{\omega_r} \tag{12.4}$$

The maximum value of θ_w, for $\theta_{on} = 0$ (zero advance angle), is given by motor design

$$\theta_{w\,max} = \theta_m = \frac{\pi}{N_r} \tag{12.5}$$

The base speed ω_b corresponds to θ_{wmax} and single voltage pulse V_d with maximum flux linkage λ_{max}, which is dependent on machine design and on the level of saturation. Thus, to increase the base speed, we have to saturate the magnetic circuit of that machine.

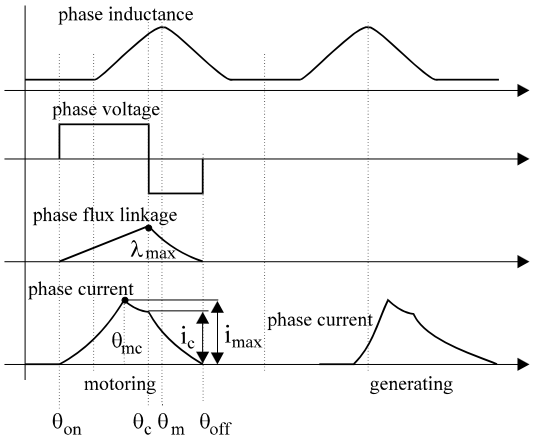

Figure 12.4. Phase inductance, voltage, flux linkage and current

For higher speeds ω_r (above ω_b), the value of θ_w may be slightly reduced but, definitely, the maximum λ_{max} has to be reduced. This is called flux weakening. Above base speed ω_b, also, the turn-on angle θ_{on} may be advanced to reach the available maximum flux λ_{max} at a smaller angle θ_c and thus allow the current to reach its maximum (at θ_{mc}) sooner and at a higher level and thus produce more torque. As a consequence, the speed/torque envelope may be enlarged. On the other hand, the turn-off process of a phase starts at $\theta_c \leq \theta_m$ and terminates at θ_{off} in the "generating" zone.

The smaller the angle $\theta_{off} - \theta_m$, the smaller the negative torque "contribution" of the phase going off. In reality, at $\theta_r = \theta_m$ (aligned position) if the current i_m is already less than (25-30%) of the peak current, the negative (generating) torque influence becomes small.

Once one phase is turned off at θ_c, another one is turned on, eventually to contribute positive torque so as to lower the total torque pulsations caused by the reduction of torque in the phase going off.

It is now evident that the entire magnetic energy of each phase is "pumped" in and out for each conduction cycle. There are mN_r cycles per mechanical revolution. A part of this energy is passed over to the incoming phase through the power electronic converter (PEC) and the rest to the DC bus filtering capacitor of PEC. Below base speed ω_b the current is limited (and controlled) through PWM (Figure 12.5).

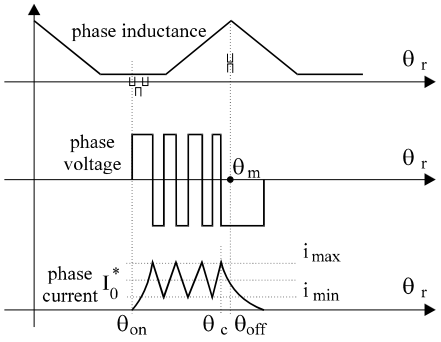

Figure 12.5. PWM below base speed

It should be noted that the interval of conduction is prolonged close to θ_m where the phase inductance is maximum. As mentioned above, at high speeds the phase turn-on angle θ_{on} is advanced and so is the turn-off angle θ_c.

12.3. AVERAGE TORQUE AND ENERGY CONVERSION RATIO

From the energy cycle point of view, based on the family of curves $\lambda(\theta_r,i)$, the two situations presented in Figures 12.4-12.5 (single voltage pulse) and, respectively, current chopping, are shown in Figure 12.6a, b, c.

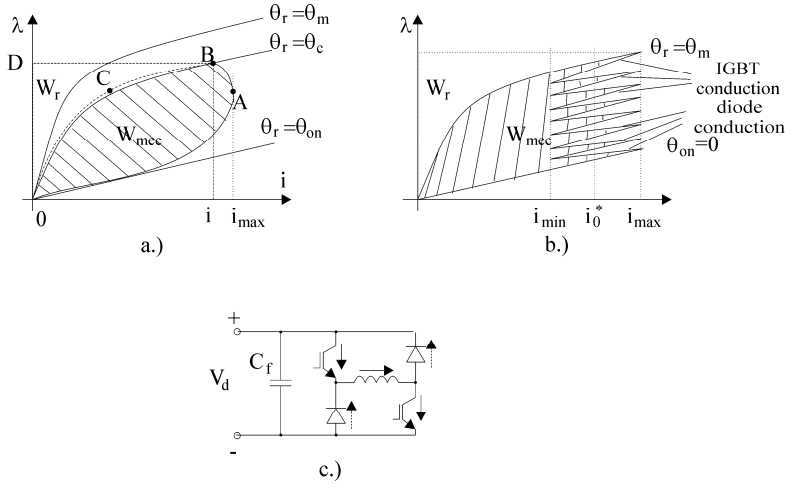

Figure 12.6. Energy cycle per phase: a.) for high speeds (one voltage pulse, Figure 12.4); b.) for low speeds (current chopping, Figure 12.5); c.) phase PEC for unipolar current per phase

The average torque T_{eav} is proportional to the hatched area in Figures 12.6 a and b, W_{mec}. Consequently, for constant speed, single phase conduction, with m phases and N_r rotor poles, the SRM average torque T_{eav} is

$$T_{eav} = \frac{W_{mec} m N_r}{\theta_c - \theta_m} \tag{12.6}$$

In parallel, an energy conversion ratio E.C. (kW / kVA) is defined as

$$E.C. = \frac{\text{Area of } \overline{OABCO}}{\text{Area of } \overline{OABDO}} = \frac{W_{mec}}{W_{mec} + W_r} \tag{12.7}$$

As the energy returned during diode conduction, W_r, is reduced by magnetic saturation, the E.C. ratio increases with saturation. Consequently, the kVA rating of the PEC (which depends on W_{mec} + W_r) is reduced by magnetic saturation. The E.C. ratio is only 0.5 for linear flux/current curves — in the absence of magnetic saturation — but it can reach values of 0.65-0.67 with magnetic saturation. Also, to keep the W_{mec} high, in comparison with the linear case, the airgap is reduced such that adequate saturation, be obtained at the same level of currents for most rotor positions. This way the level of average torque can be maintained.

Note that the maximum flux per phase and the maximum inductance are reduced by magnetic saturation. Current commutation becomes faster, while the base speed for a given voltage is also increased.

Further increase in the E.C. ratio may be obtained through DC premagnetization by a diametrical coil (Figure 12.1a) in series with all phases [3].

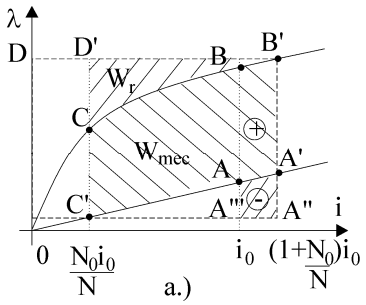

Figure 12.7. Energy cycle with DC premagnetization

The energy cycle is moved to the right (Figure 12.7) with the equivalent current i_0N_0 / N (N_0 - turns in the premagnetization coil, N - turns in the phase coil). The mechanical energy is increased by the area AA′B′B minus area AA′A″A‴, while the energy retrieved during phase demagnetization, W_r, is reduced by the area OCD′D. Consequently, the energy conversion

ratio E.C. is notably increased (from 0.64 to 0.74, [3]) at the price of the losses in the premagnetization coil (19% additional copper losses, [3]).

12.4. THE PEAK kW/kVA RATIO

The peak kW/kVA ratio [4] is

$$\text{peak kW/kVA} = \frac{\alpha_s N_r Q}{8\pi} \tag{12.8}$$

where α_s is the stator pole pitch ratio (α_s = 0.4-0.5), and Q is

$$Q \approx C\left(2 - \frac{C}{C_s}\right) \tag{12.9}$$

where C is the ratio between the turn-on angle below the stator pole and the stator pole angle β_s.

In general, C = 1 at zero speed and decreases down to C = 0.65 at base speed.

Also,
$$C_s = \frac{\lambda_u - 1}{\lambda_u \sigma - 1};\ \ \lambda_u = \frac{L_a{}^u}{L_u} \approx (4 \div 10);\ \ \sigma = \frac{L_a{}^s}{L_a{}^u} \approx (0.3 \div 0.4) \tag{12.10}$$

L_u is the unaligned inductance, and $L_a{}^u$ and $L_a{}^s$ are the aligned unsaturated and saturated values of phase inductance, respectively.

The peak apparent power, S, of switches in the converter is

$$S = 2mV_d I_{peak} \tag{12.11}$$

where V_d is the DC source voltage and I_{peak} is the peak current value.

For an inverter-fed IM drive the peak kW / kVA is

$$(\text{peak KW/KVA})_{IM} = \frac{3}{\pi}\frac{V_d I \cdot PF}{K(6V_d I)} = \frac{3}{\pi}\frac{PF}{6K} \tag{12.12}$$

where K is the ratio between the peak current I_{peak} and the peak value of the current fundamental in IMs when inverter-fed (for the 6 pulse mode K = 1.1-1.15); PF is the power factor.

Example 12.1.

For a 6 / 4 SRM with $\sigma = L_a{}^s / L_a{}^u = 0.4$, $\lambda_u = L_a{}^u / L_u = 6$, C = 1, α_s = 0.4, calculate the peak kW / kVA ratio.

Solution:

As $\sigma = 0.4$ and $\lambda_u = 6$, the coefficient C_s (from 12.10) is

$$C_s = \frac{\lambda_u - 1}{\lambda_u \sigma - 1} = \frac{6 - 1}{6 \cdot 0.4 - 1} = \frac{5}{1.4} = 3.57 \tag{12.13}$$

Further on from (12.9) Q is

$$Q = C\left(2 - \frac{C}{C_s}\right) = 1\left(2 - \frac{1}{3.57}\right) = 1.72 \tag{12.14}$$

Consequently, from (12.8)

$$\text{peak kW/kVA} = \frac{\alpha_s N_r Q}{8\pi} = \frac{0.4 \cdot 4 \cdot 1.72}{8\pi} = 0.1095 \tag{12.15}$$

For an induction motor with P.F. = 0.85 and K = 1.12

$$(\text{peak kW/kVA})_{IM} = \frac{3}{\pi}\frac{0.85}{6 \cdot 1.12} = 0.1208 \tag{12.16}$$

So, in terms of the PWM inverter rating, the IM (with rather good power factor) is only 10-20% better than the PEC for the equivalent SRM which is supposed to produce the same power at the same efficiency.

12.5. THE COMMUTATION WINDINGS

The turn-off process angle (time) θ_c–θ_{off} has to be limited. In general, θ_c–$\theta_{off} < \beta_s$ (β_s is the stator pole angle) is not sufficient, as a strong negative (generating) torque may occur.

Conversely, in the generator mode, the turn-on process has to be advanced within motoring regime (positive inductance slope), but not too much, in order to avoid strong motoring torque influences.

For both cases and all speeds θ_{off}–θ_m < 3-4 degrees. Through advanced saturation (reduced airgap) and the advancing of turn-on and turn-off angles θ_{on} and θ_{off}, the turn-off interval angle θ_{off}–θ_m may be kept (up to a certain speed) below the challenging limits at the price of higher torque pulsations.

If the diametrical coil (proposed for demagnetization) - Figure 12.1a - is turned on whenever an active phase is de-energized, the magnetic energy will be passed to this commutation phase, partly. After the current is zero in the going-off phase, the commutation winding is turned off. Notably smaller turn-off times are obtained this way (Figure 12.8) [5].

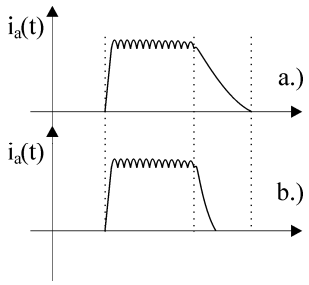

Figure 12.8. Current profile: a.) conventional,
b.) with commutation coil (winding)

The effect of the commutation current turn-off process is evident but we have to consider that an additional coil with an additional phase in the PEC and the corresponding losses make the price for the improvement thus obtained. The energy conversion rate CE is also increased by a few percent. Finally, the interaction of the commutation winding with, say, a faulty (short-circuited) phase notably reduces the fault tolerance claims of conventional SRM. Other distributed winding arrangements for SRMs have been proposed [6,7] for increasing the torque density (Nm/kg of rotor), but they all seem to impede on the fault tolerance claims of conventional SRMs, while the efficiency is not increased either.

In what follows we will deal with modeling, digital simulation and the control of the basic 6 / 4 and 8 / 6 SRMs as they are most representative.

12.6. SRM MODELING

The mathematical model of SRM is highly nonlinear due to magnetic saturation influence on the $\lambda(\theta_r,i)$ curve family, but it allows for phase-torque superposition as the interaction between phases is minimal.

As SRM has double saliency, stator (phase) coordinates are mandatory.

The phase equations are

$$V_{a,b,c,d} = r_s i_{a,b,c,d} + \frac{d\lambda_{a,b,c,d}\left(\theta_r, i_{a,b,c,d}\right)}{dt} \tag{12.17}$$

with the family of curves $\lambda_{a,b,c,d}(\theta_r,i_{a,b,c,d})$ obtained for one phase only (as the periodicity is π / N_s). These curves may be obtained either through theory or through tests. Analytical or finite element methods are used for the scope. Accounting for magnetic saturation and airgap flux fringing is mandatory in all cases.

The motion equations are:

$$J\frac{d\omega_r}{dt} = T_e - T_{load}; \quad \frac{d\theta_r}{dt} = \omega_r \tag{12.18}$$

with

$$T_e = \sum_{a,b,c,d} T_{e_{a,b,c,d}}; \quad T_{e_{a,b,c,d}} = \frac{\partial}{\partial\theta_r}\int_0^{i_{a,b,c,d}} \lambda_{a,b,c,d}\left(\theta_r, i_{a,b,c,d}\right) di_{a,b,c,d} \tag{12.19}$$

Let us use the subscript i for one dominating phase.

Equation (12.16) may be written as

$$V_i = r_s i_i + \frac{\partial\lambda_i}{\partial i_i}\frac{di_i}{dt} + \frac{\partial\lambda_i}{\partial\theta_r}\frac{d\theta_r}{dt} \tag{12.20}$$

Denoting $\frac{\partial\lambda_i}{\partial i_i}$ as the transient inductance L_t:

$$L_t\left(\theta_r, i_i\right) = \frac{\partial \lambda_i\left(\theta_r, i_i\right)}{\partial i_i} \tag{12.21}$$

The last term in (12.20) represents the back e.m.f. E_i

$$E_i = \frac{\partial \lambda_i}{\partial \theta_r} \cdot \omega_r \tag{12.22}$$

So (12.20) becomes

$$V_i = r_s i_i + L_t\left(\theta_r, i_i\right)\frac{di_i}{dt} + E_i\left(\omega_r, \theta_r, i_i\right) \tag{12.23}$$

An equivalent circuit with time-dependent parameters may be defined based on (12.23) - (Figure 12.9).

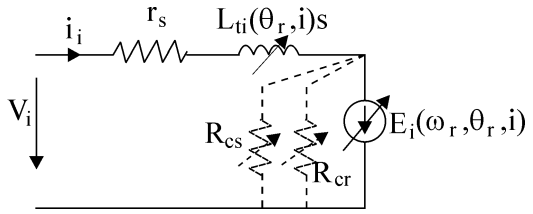

Figure 12.9. Equivalent circuit of SRM with core losses accounted for

The core losses are represented by the variable resistances in parallel with the e.m.f. E_i, based on the assumption that only the main flux produces core losses. Core losses occur both in the stator and in the rotor core as this machine does not operate on the traveling field principle [9,10].

Especially in high speed applications (above 6000 rpm) core loss has to be considered not only for efficiency calculations but also in the transient current response assessment.

Note: Only for the linear case (no magnetic saturation) the instantaneous torque $T_e(t)$ is

$$T_e(t) = \sum \frac{1}{2}\frac{E_i\left(\omega_r, \theta_r, i_i\right)\, i_i}{\omega_r} \tag{12.24}$$

As usually, heavy magnetic saturation is present, $E_i\left(\omega_r, \theta_r, i_i\right)$ as in (12.22) is a pseudo e.m.f. as it also includes a part related to the magnetic energy storage. Consequently, the torque is to be calculated only from the coenergy formula.

For more details on this aspect, see [11].

12.7. THE FLUX-CURRENT-POSITION CURVE FITTING

For digital simulations and control purposes the $\lambda_i(\theta_r,i)$ curves family has to be known. The safest way is to use measurements — at standstill or with the machine in rotation. Finite element calculations represent the second best approach. Once this is done what still remains is to determine the inverse function $i(\lambda_i,\theta_r)$ and, eventually, $\theta_r(\lambda_i,i_i)$. There are two main ways to invert the $\lambda_i(\theta_r,i)$ to find either $i(\lambda_i,\theta_r)$ or $\theta_r(\lambda_i,i_i)$.

One way is to use analytical functions (polynomials or exponentials) [12,13]. The second way is to use direct approximations, for example, fuzzy logic [14] or other curve fitting methods. For digital simulations the computation time is not so important. In the case of control, torque calculation, $T_{ei}(\lambda_i,\theta_r,i_i)$, or position estimation, $\theta_r(\lambda_i,i_i)$, is done on line.

Using exponential approximations [12,13] the phase flux linkage $\lambda_i(\theta_r,i)$ is

$$\lambda\left(\theta_r,i\right)=a_1\left(\theta_r\right)\left(1-e^{-a_2\left(\theta_r\right)i}\right)+a_3\left(\theta_r\right)i \tag{12.25}$$

The periodicity of λ is built in the $a_{1,2,3}(\theta_r)$ functions expressed as Fourier series

$$a_m=\sum_{k=0}^{\infty}A_{mk}\cos\left(k\alpha\theta_r\right) \tag{12.26}$$

$\alpha = 4$ for a 6/4 machine and $\alpha = 6$ for an 8/6 machine. A_{mk} is the Fourier coefficient of k^{th} order in a_m.

Other rather cumbersome analytical functions of current, based on linear position dependence approximations, are also feasible [15].

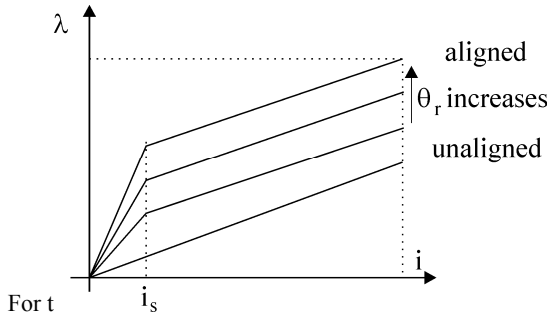

Figure 12.10. Linear $\lambda(\theta_r,i)$ approximations

It is supposed that magnetic saturation occurs at the constant current level i_s irrespective of rotor position. As the airgap is small, in heavily saturated motors, the local overlapping pole zone may saturate quickly. Thus the flux linkage varies linearly with rotor position. It is known, however, that

close to the aligned position such an approximation model seems less adequate

$$\lambda = i\left(L_u + \frac{K_s\left(\theta_r - \theta_0\right)}{i_s}\right); \quad i \le i_s \tag{12.27}$$

$$\lambda = L_u i + K_s\left(\theta_r - \theta_0\right); \quad i \ge i_s \tag{12.28}$$

where L_u is the unaligned inductance value, K_s is the only coefficient to be found from the family of $\lambda(\theta_r,i)$ curves — eventually one intermediate position information suffices; θ_0 is the position angle of the pole entry end; $\theta_{nmax} = \theta_m$ — the pole exit end position angle.

12.8. SRM DRIVES

SRM drives may be classified with respect to a few criteria:

- with motion (position, speed) sensors;
- without motion sensors (sensorless).

They also may be:

- general — for low dynamics applications (moderate speed range and costs);
- high grade (performance) — for servos.

They differ in complexity, cost and performance. Performance is defined by the energy conversion ratio, speed control range, precision and quickness of torque response.

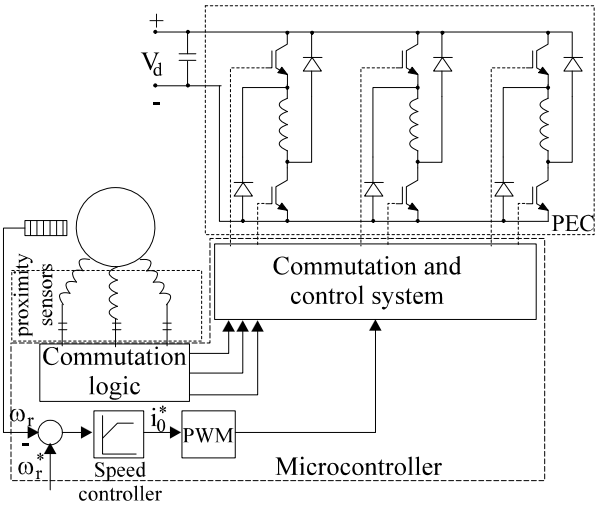

Figure 12.11. Basic (historical) SRM drive

Servo applications require precise speed or position control and fast torque response (in the milliseconds range). Historically, for low cost SRM drives, proximity (Hall) position sensors have been used to trigger the turn-off conducting phase and at the same time, turn-on of the incoming phase. For constant speed only, even the position angle between two proximity sensors signals may be estimated.

Consequently, advancing the turn-on and turn-off angle may be performed in such drives only for steady-state or low dynamics.

Also, starting under load poses problems because, from the three (four) proximity sensor signals, we may only infer what phase has to be turned on but not exactly the initial position. A separate speed signal is necessary for safe starting under load.

In the following section we will discuss an up-to-date general drive, a high grade drive with precision (encoder) position feedback and an advanced motion-sensorless drive.

12.9. GENERAL PURPOSE DRIVE WITH POSITION SENSOR

For applications with wide speed range but moderate energy conversion or dynamic performance, a precision position sensor is used to commutate the phases at speeds down to a few rpm. No speed sensor is used (Figure 12.12).

The core of the general purpose SRM drive in Figure 12.12 is the dependence of the turn-on θ_{on} and turn-off θ_{off} angles (for motoring and generating) on speed. A linear dependence is the obvious choice.

We may distinguish three regions:

- the low speed - constant torque - zone: θ_{on} = cons., θ_{off} = cons., $\omega_r < \omega_b$;
- the constant power zone, $T_e\omega_r$ = cons.: θ_{on} and θ_{off} decrease with speed $\omega_r > \omega_b$;
- the $T_e\omega_r^2$ = cons. zone, above ω_{m1} (Figure 12.13a)

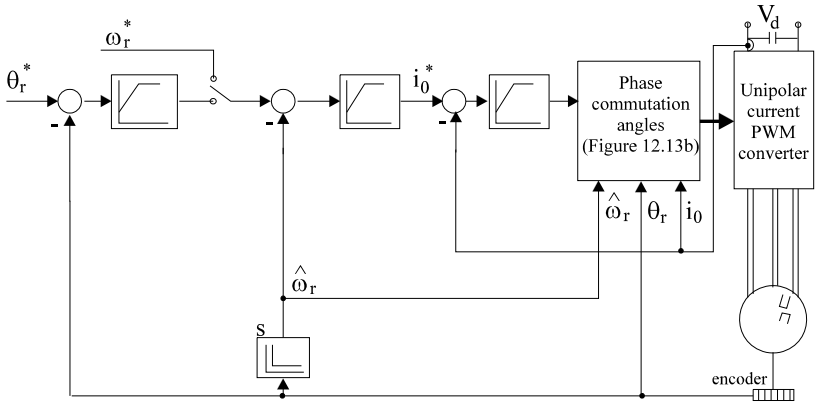

Figure 12.12. General purpose SRM drive with encoder

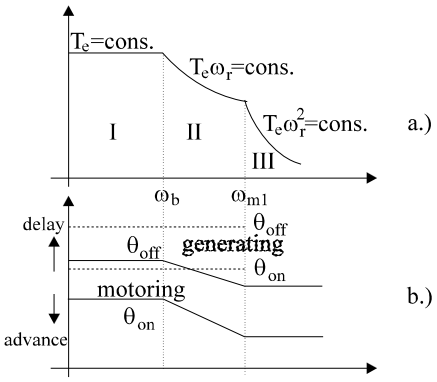

Figure 12.13. a.) Torque/speed zones, b.) turn-on and off angles θ_{on} and θ_{off} for motoring and generating

The above control philosophy assumes flat top currents below base speed, obtained through closed-loop (current control) PWM and single-voltage pulses above base speed when (and if) current control is no longer feasible due to lack of voltage reserve (the e.m.f. overcomes the DC link voltage V_d).

As is easy to see, no complicated data on machine flux/current/position curves is necessary as $(\theta_{on})_{min}$ and $(\theta_{off})_{min}$ are to be obtained through trial and error. For more details on such a drive see [16].

The drive could produce moderate performance over a wide speed range but quick torque response optimum energy conversion or maximum torque/speed envelope is not guaranteed.

However, there are many applications when the general purpose SRM drive suffices.

Example 12.2.

A 6 / 4 three-phase SRM has the following data: $\beta_s = \beta_r = 30°$ (stator and rotor pole angle), $J = 0.002 kgm^2$, maximum current $i_{omax} = 10A$, DC voltage $V_d = 300V$, $r_s = 1.5\Omega$, maximum flux (aligned position) $\lambda_{max} = 0.8Wb$, minimum flux $\lambda_{min} = 0.16Wb$, linear flux/current curves (12.27-12.28) are supposed, with $i_s = 2A$ (Figure 12.10).

A position sensor with 1024 pulses per revolution is available.

Calculate:

- the unaligned inductance, K_s coefficient in (12.27-12.28) and the maximum average torque available for $i_{max} = 10A$ at zero speed.
- using Matlab/Simulink run digital simulations on a general purpose SRM drive (Figures 12.14-12.17) and choose the turn-on and -off angles to explore starting transients, step load and step-speed responses.

Solution:

At zero speed the conduction angle $\theta_{rmax}-\theta_0 = \beta_s = 30^0 = \pi / 6$ with $\theta_0 = 0$, for the aligned position $\theta_{rmax} = 30°$.

In the unaligned position $\theta_r = \theta_0$ and from (12.27)

$$\lambda_{min} = i_{max} L_u \tag{12.29}$$

So the unaligned inductance L_u is

$$L_u = \frac{\lambda_{min}}{i_{max}} = \frac{0.16}{10} = 0.016 \quad \text{H} \tag{12.30}$$

Also, from (12.28) λ_{max} is

$$\lambda_{max} = i_{max} L_u + K_s \beta_s \tag{12.31}$$

$$K_s = \frac{0.8 - 0.16}{\pi / 6} = 1.223 \quad \text{Wb/rad} \tag{12.32}$$

Simulation results on a SRM motor drive with PEC are presented. The motor model was integrated in a block (SRM in Figure 12.14).

Changing motor parameters is done by clicking on this block. A dialog box appears and you may change them by modifying their default values.

The drive system consists of PI speed controller ($K_i = 10$, $T_i = 0.05$s), motor block (voltage equations for each phase, motion equations, (12.18-12.20), angle selection and advancing block, and three blocks (A, B, C) for matrix calculation (as functions of θ_r and phase current): Equations (12.33-12.35).

$$\frac{\partial \lambda_i}{\partial i_i} = \begin{bmatrix} L_u & L_u \\ L_u + \frac{K_s}{i_s}(\theta_r - \theta_0) & L_u \\ L_u + \frac{K_s}{i_s}(\theta_0 + \pi/3 - \theta_r) & L_u \end{bmatrix} \tag{12.33}$$

$$\frac{\partial \lambda_i}{\partial \theta_r} = \begin{bmatrix} 0 & 0 \\ \frac{K_s}{i_s} i_i & K_s \\ -\frac{K_s}{i_s} i_i & -K_s \end{bmatrix} \tag{12.34}$$

$$\frac{\partial\left(\int \lambda_i di_i\right)}{\partial\theta_r} = \begin{bmatrix} 0 & 0 \\ \frac{K_s}{2i_s} i_i^2 & K_s i_i \\ -\frac{K_s}{2i_s} i_i^2 & -K_s i_i \end{bmatrix} \tag{12.35}$$

Each line of these matrices represents a case function of phase inductance for 3 operation modes (see Figure 12.2) based on (12.27 and 12.28). The columns represent the two cases for $i \le i_s$ and $i \ge i_s$.

The angle selection and advancing block produce the voltage PWM between θ_{on} and θ_c angles and, respectively, negative voltage supply until θ_{off} (where the current for the working phase becomes zero); see Figure 12.5. In this block the firing angle is selected for each phase as a function of rotor position information.

The study examines the system's behavior for starting, load perturbation, motoring and generating of the SRM drive.

The integration step (50μs) can be modified from the Simulink's *Simulation/Parameters*.

To find out the structure of each block presented above, unmask them (*Options/Unmask*). Each masked block contains a short help screen describing that block (inputs/outputs/parameters).

The block diagram of the electric drive system is presented in the Figure 12.14.

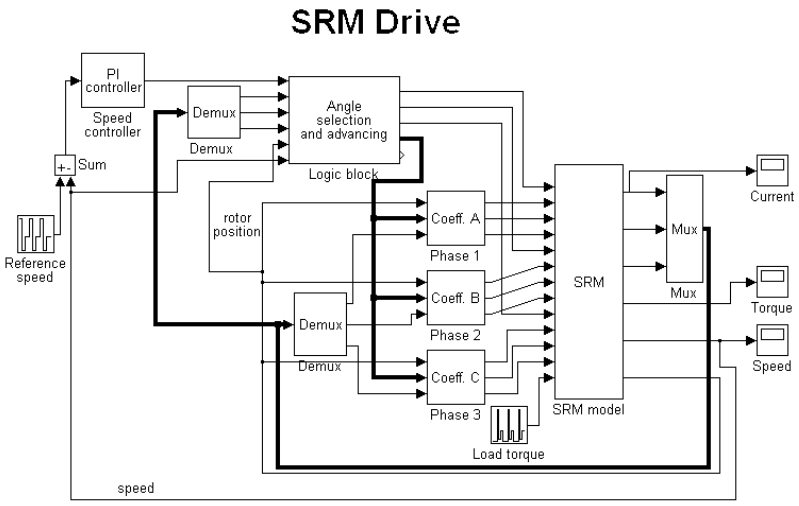

Figure 12.14. Block diagram of simulated SRM drive

The following Figures represent the speed (Figure 12.15), torque (Figure 12.16) responses, and current waveforms (Figure 12.17) for speed step response from 0 to 700 rad/s (advancing angle is 5^0 after 500rad/s), changing the speed reference at 0.3s (from 700rad/s to 150rad/s; the machine is working as a generator until it reaches the reference speed), load torque is applied at 0.5s (8Nm), unloading is done at 0.6s; and, at the same time, the speed reference is changed to 400rad/s and loading is done again at 0.8s (3Nm).

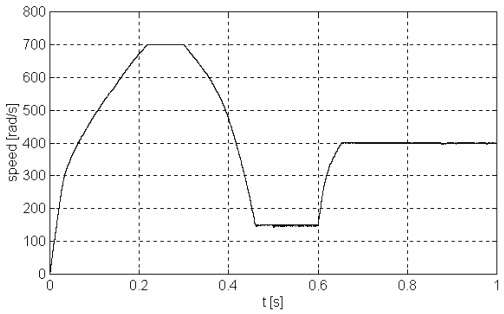

Figure 12.15. Speed response

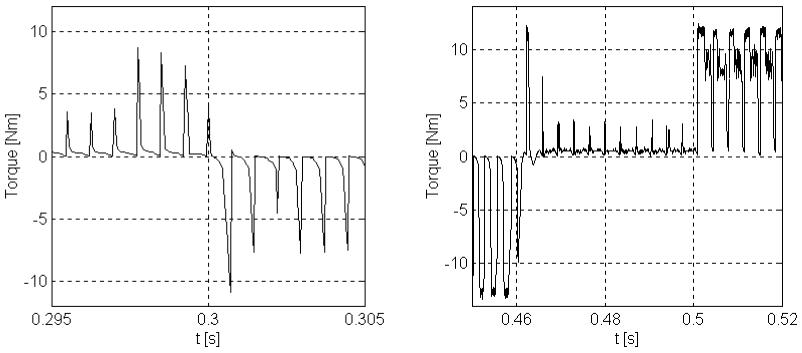

a.) b.)

Figure 12.16. Torque response

12.10. HIGH GRADE (SERVO) DRIVES

High grade (servo) drives have a strong capability for position, speed or torque control, characterized by high energy conversion ratios, precision, robustness and quickness of torque control and rather wide speed range control. Traditionally, DC brush, brushless (PMSM) or (recently) advanced control IM drives are used as servos.

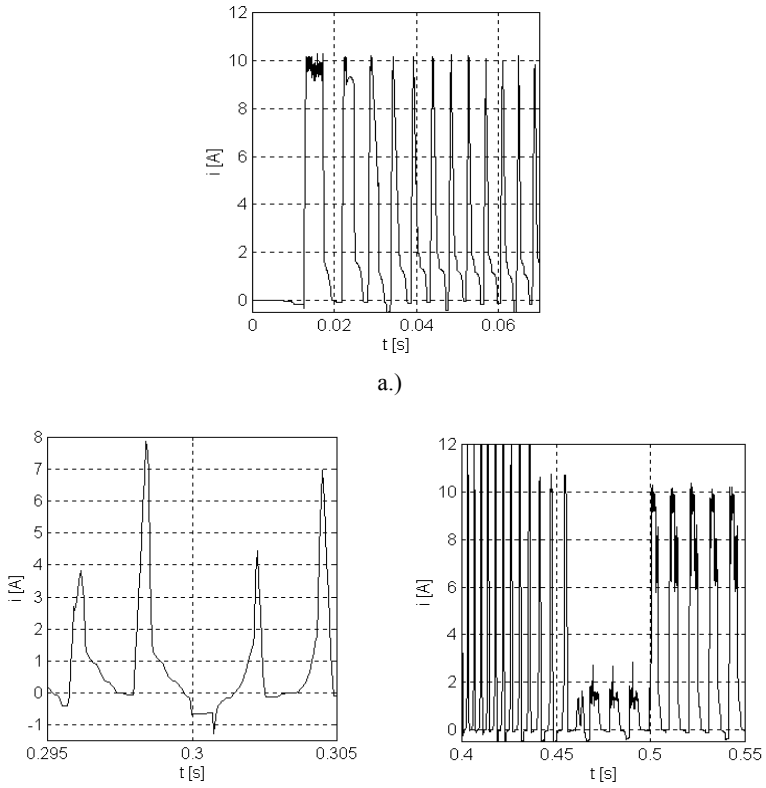

Figure 12.17. Current waveforms for the transients in Figure 12.15

The strong nonlinearity in the flux/current/position and torque/current/ position curves makes, in principle, the SRM apparently less attractive for servos. However the motor simplicity and ruggedness in such applications may not be overlooked.

An attempt to build a SRM servo drive may start with a revisitation of torque production in the SRM.

a. Torque sharing and current shaping

In servos torque pulsations should be reduced to less than 1% of rated torque if smooth (precise) torque control is to be obtained. If only one phase can produce torque (positive inductance slope) at any time, chances to reduce the torque pulsations are low, especially if winding losses are to be limited.

A 4-phase (8/6) SRM has two phases capable of producing torque at the same time, while, in a three-phase machine, only one phase can produce torque at any time. Consequently, 4 phases seem necessary for servo performance. In this case, single-phase torque production will be alternated

with two-phase torque action for low losses or low torque pulsations. The total torque T_e is the sum of the torques per phase T_{ei} (Figure 12.18)

$$T_e = \sum_{i=1}^{m} T_{ei}\left(i_i, \theta_{ri}\right); \quad i = 1,\ldots,m; \; m = 4 \tag{12.36}$$

The torque response time is basically equal to the time to reach the maximum flux level in the machine and it is in the order of milliseconds for the kW power range.

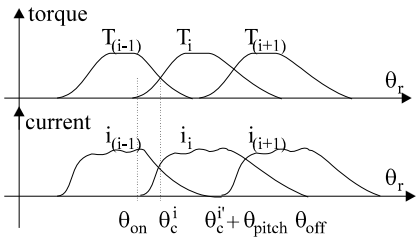

Figure 12.18. Phase torque components and phase current shaping

How to turn on and off various phases and profile the current waveforms to minimize torque ripple is not a problem with a unique solution.

A second condition is required. To determine the flux/torque relationships for SRMs we may apply two optimization criteria for torque sharing:

- maximum torque per unit winding losses (below base speed);
- maximum torque per unit admissible flux level (above base speed)

For both criteria the crucial problem is when to switch from one phase to the next. In [17] the switch over angle θ_c^i (for the first criterion) and θ_c^λ (for the second) are chosen so that in these conditions the values of torque are equal to each other (half the reference torque: $T_e^* / 2$) and so are the currents (Figure 12.18), and the flux levels.

The θ_{on} angle is calculated to allow the current rise required in the machine characteristics. Before θ_c^i (θ_c^λ), the phase with stronger torque was in charge, while after that the incoming phase predominates in torque production.

The problem is how to find the current versus position profiles for various speeds and reference torques. This task definitely requires a thorough knowledge of the $\lambda(i,\theta_r)$ curves which have to be inverted to produce $i_i(\omega_r, T_i, \theta_r)$ functions. Various mathematical approximations of $\lambda_i(i_i,\theta_r)$ functions determined through tests may be used for the scope [17]. Here is an example

$$\lambda\left(i, \theta_k\right) = a_0\left(\theta_k\right)\tan^{-1}\left(a_1 i\right) + a_2\left(\theta_k\right)\, i \tag{12.37}$$

where θ_k are discrete rotor positions.

From the co-energy formula the corresponding torque is computed. The torque sharing functions may be implemented in a feedforward manner in the sense that four reference currents and current controllers make sure that the reference currents are closely tracked (Figure 12.19).

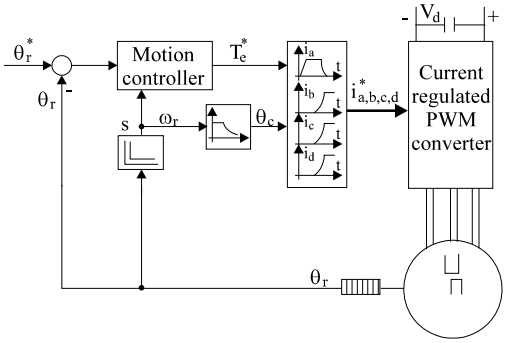

Figure 12.19. High grade SRM drive with feedforward torque sharing optimization

To store all the waveforms for various speeds would require much memory and thus, in [17], only the waveforms for maximum speed are stored. For lower speeds the phase voltage (flux) available is not surpassed.

It may be seen from Figure 12.19 that the switch over angle θ_c (θ_c^i at low speeds and θ_c^λ at high speeds) has to be precalculated based on the optimization criteria mentioned above. In general, $\theta_c^i > \theta_c^\lambda$ as expected.

Torque pulsations of less than 4% from 0.5rpm to 5000rpm and good positioning performance have been reported in [17, 18]. Also, it has been shown that the maximum torque/loss criterion produces more power at low speeds while the maximum torque/flux enlarges the constant power speed/torque envelope.

Still not solved satisfactorily is the self-commissioning mode when the drive itself, before calibration, should gather and process all the data for the $\lambda(\theta_r,i)$ curve family within one minute as is done currently for a.c motor drives.

12.11. SENSORLESS SRM DRIVES

Sensorless SRM drives may be open-loop or closed-loop with respect to speed (or position) control. Open-loop sensorless driving implies fixed dwell angle $\theta_w = (\theta_c - \theta_{on})$ control with synchronization as is done in stepper motors [18] (Figure 12.20). Increasing the dwell angle tends to increase the stability but with lower efficiency. To solve this problem the dwell angle is increased with DC link current (load in general). Though simple, such a method has stability problems, produces low dynamics and allows for a limited speed control range.

Consequently, open-loop sensorless drive solutions seem today of some historical importance but hardly practical.

Closed-loop sensorless SRM drives have been proposed to compete with the, by now, commercial sensorless AC drives capable of at least 100 to 1 speed range and torque response in the milliseconds range with good speed precision (less than 0.2-0.3% of rated speed).

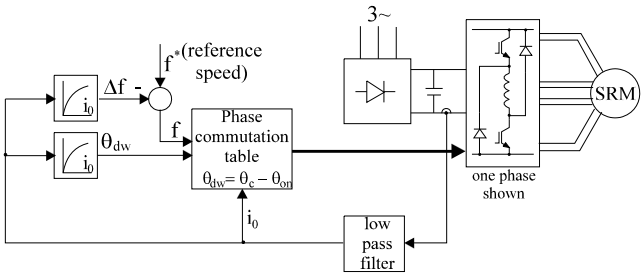

Figure 12.20. Basic open-loop sensorless SRM drive

Competitive closed-loop sensorless SRM drives should be high grade and, in addition, capable of producing, through estimation (or observation) the rotor position $\hat{\theta}_r$ and speed $\hat{\omega}_r$ with good precision, robustness and on time (fast). Among the closed-loop strategies for position and speed estimation we mention the incremental inductance estimator in the active phase, diagnostic pulse injection in the activated or passive phase, mutual inductance estimation, observers, etc. For a collection of papers on these solutions see [19] section 4.

To the best of our knowledge, no close loop sensorless SRM drive has reached the markets as of this writing. We will dwell only a little on two promising solutions: the combined voltage-current-model-based [20] and the fuzzy logic (rule-based) observers [14].

12.12. THE VOLTAGE-CURRENT MODEL-BASED POSITION SPEED OBSERVER

Basically, the phase voltages and currents are measured with wide-band frequency sensors with optoisolation and analog-digital fast (2μs or so) converters. In any case, the $\lambda(\theta_r,i)$ family of curves has to be *a priori* measured or FEM calculated and curve fitted through derivable functions.

The voltage model is represented by the stator phase equations

$$\frac{d\lambda_i}{dt} = V_i - r_s i_i \tag{12.38}$$

This model may be used to estimate the flux, but for low speeds, the model is erratic due to integration drift, voltage and current measurements noise and stator resistance variation with temperature.

From the $\lambda(\theta_r,i)$ curves, with current measured and $\hat{\theta}_r$ estimated in a previous time step, we may estimate back the current $\hat{i}_i$ with the current error $\Delta i_i(k)$. A position correction $\Delta\theta_r(k)$ is operated to drive this error to zero. Thus the voltage and current models have already been used together once [20]

$$\Delta\theta_i(k) = -\left(\frac{\partial\lambda_i}{\partial i_i}\right)\Delta i_i(k) \Big/ \frac{\partial\lambda_i}{\partial\theta_r(k)} \tag{12.39}$$

The three position corrections (from all three-phases) may be averaged (or weighted) to give

$$\Delta\theta_r = \frac{(\Delta\theta_a + \Delta\theta_b + \Delta\theta_c + \ldots)}{m} \tag{12.40}$$

Thus the estimated position $\theta^e(k)$ is

$$\theta^e(k) = \theta_p(k) + \Delta\theta_r \tag{12.41}$$

where $\theta_p(k)$ is the value estimated in the previous time step.

Now, with a new position $\theta^e(k)$ and the predicted flux values from the voltage model, once again new currents are estimated and new current errors $\Delta' i_i$ appear. Flux corrections $\Delta\lambda_i(k)$, based on $\lambda(\theta_r,i)$ curves, are

$$\Delta\lambda_i = \frac{\partial\lambda_i}{\partial i_i}\Delta' i_i \tag{12.42}$$

$$\Delta\lambda_i(k) = \lambda_i(k) + \Delta\lambda_i \tag{12.43}$$

Finally, the rotor position is predicted using its estimated values at three time steps K–2, K–1, K and a quadratic prediction [20]

$$\theta^p(k) = 3\theta^e(k) - 3\theta^e(k-1) + \theta^e(k-2) \tag{12.44}$$

The flux correction reduces the integrator drift. Mechanical load parameters are not required and the magnetic saturation is included through the $\lambda(\theta_r,i)$ curves. Still, the speed estimator (from position) is to be added. It has to be noted that a great number of calculations is required. A TMS310C31 DSP may provide for a 100μs computing (and control) cycle. Good results, for position control only, have been reported, down to 30rpm, in [20].

The control system for the high grade SRM drive has to be added to the voltage-current model position (and speed) observer (Figure 12.21) to produce a high performance SRM drive.

Fuzzy logic may also be used to realize a voltage-current observer similar to that presented in this section.

In essence, the $\lambda(\theta_r,i)$ curve family is approximated (fitted) through the fuzzy logic approach, avoiding analytical approximations as above. Digital simulations have shown [14] such a system capable of position estimation with an error less than 0.4 degree.

Alternatively, sliding mode rotor position and speed estimators based on given $L_s(\lambda_s, \theta_r)$ curves, with flux estimator, has been also proven to produce good motion sensorless control [21] for a 5:1 constant power range by switching from maximum torque/current to maximum torque/flux optimal turn on θ_{on} and turn off θ_{off} phase angle estimation. High torque dynamic response has been also demonstrated with direct average torque control and on-line correction of off-line reference current and reference θ^*_{on} and θ^*_{off}, based on PI torque error output [22].

For more on position-sensorless control see Refs [23 - 25].

The first sensorless 100 to 1 speed range (and 0.3% of rated speed error and quick torque response SRM drive) is apparently still due.

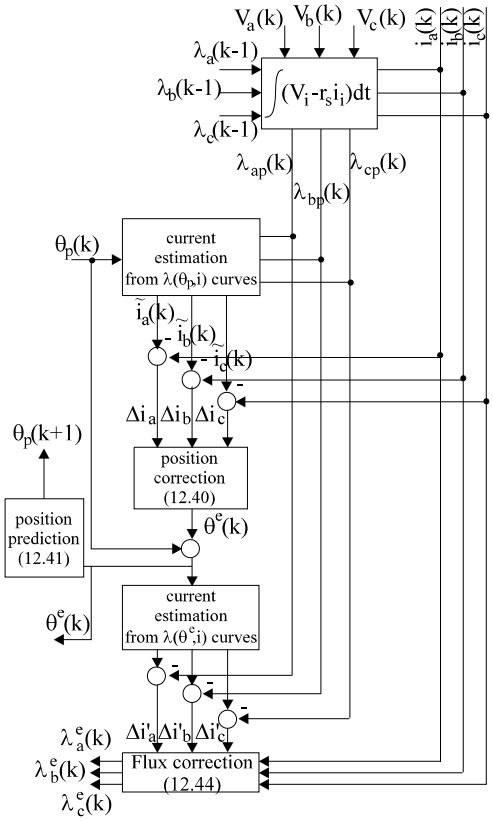

Figure 12.21. Voltage-current model position observer

12.13. SINGLE-PHASE SRM CONTROL

The single phase SRM with equal count of stator and rotor poles (2/2 or 4/4) and self starting parking position provision seems very attractive for home appliances or automotive actuators below 1Nm of torque because of the possibility of utilizing only one active power switch; that is, a lower cost drive is obtained.

In addition, with 6/6, 4/4, and even 2/2 stator/rotor pole count, the single phase SRM may be designed in some conditions for more torque density than a three phase SRM, which is characterized, anyway, by one phase acting at any time.

The self-starting parking position may be obtained by:

- Parking PMs on top of special poles (Figure 12.21a)
- Step airgap under the stator poles $g_2 / g_1 = 1.5 - 2.5$ (Fig. 12.21b) or snail cam rotor shape.
- Magnetic saturation of roughly one half of the rotor poles with the other half providing a double airgap $g_2 \sim 2g_1$ (g_1 airgap under the saturable zone – Figure 12.21c) [26].

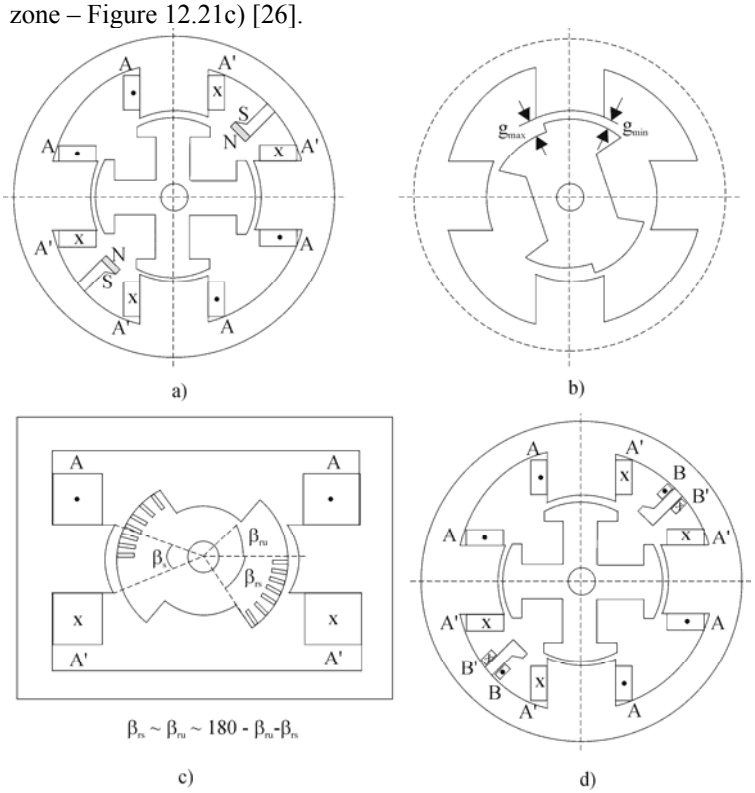

Figure 12.21. Self starting parking position methods: a) parking magnet, b) stepped airgap, c) saturated half rotor pole plus stepped airgap, d) energy-drain starting phase.

- With an additional starting phase that is automatically turned on when the active phase turns off, some additional torque is produced by the auxiliary phase even during operation at nonzero speed (Figure 12.21d) [27, 28].

Basically all methods of providing self starting position allow for unidirectional motion from standstill.

However once the motor starts in one direction, in presence of two Hall sensors (in general), it is feasible to brake the rotor regeneratively and then rotate it in the reverse direction of motion. This way bidirectional (or four quadrant) motion is claimed with single phase SRM [28].

A basic power electronics converter for the single phase SRM without and with starting phase is shown in Figure 12.22.

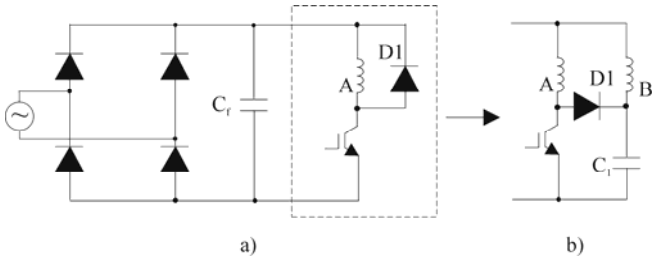

Figure 12.22. Single IGBT (MOSFET) converter: a) for single phase SRM, b) for single phase SRM with energy-drain starting phase

The single phase SRM main winding A works only during about half the time as only then the torque is unidirectional (positive or negative).

However, the saturated rotor half – pole with stepped airgap configuration (Figure 12.21c) claims that the motoring cycle (negative torque) may be wider than the generating one (Figure 12.23).

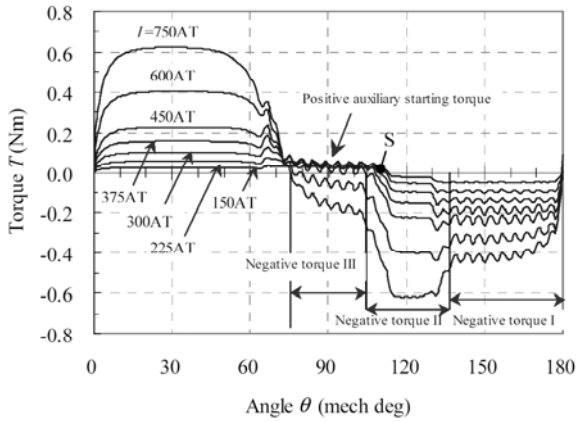

Figure 12.23. Torque cycle of single phase SRM of Figure 12.21c

There are two zero torque positions at 75° and, respectively, 110° besides the zero and 180° ones. Moreover, for low current the torque between 75° and 110° is positive, while for large current it is negative (motoring).

If the rotor is positioned for θ_r=75°, then, with a small current, the rotor is moved to θ_r=110° in the opposite direction of desired motion.

Further on, with high current (at 110° rotor position) the large negative torque should be able to move the rotor to the left till θ_r=0, when again negative torque is available, to continue motor acceleration.

Playing with magnetic saturation zone (made of slots and teeth on the rotor half-pole), the starting torque at low current may be increased to 10% of rated torque, to handle easy starts. Heavy starts are, apparently, hardly possible.

On the other hand, with the starting phase B present (Figure 12.21d), if the rotor is initially aligned to the main phase A poles, a current pulse does not move the rotor, but, when the phase A is turned off, the energy is drained through the starting phase B, tending to align the rotor to its axis. This way, when the second voltage pulse is applied to the main phase, the latter should provide for motor self-starting from the starting phase axis towards main phase axis. Once the motor starts in the preferred direction of motion, and two Hall proximity sensors are available, the motor may be regeneratively braked and then controlled (on the fly) to accelerate in the opposite direction of motion (Figure 12.24). Four quadrant operation is thus claimed [28].

A nonhesitant heavy (direct) bidirectional motor start does not seem possible even with this solution.

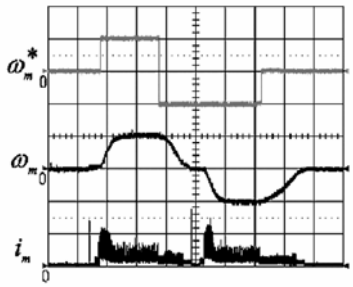

Figure 12.24. Four quadrant operation 15000 rpm/div and 5s/div

12.14. SUMMARY

- SRM is a single or multiphase doubly salient simple and rugged electric motor with a passive (windingless) rotor.
- The SRM phases are fed sequentially with voltage pulses through a sort of PWM.
- Phase commutation is rotor position dependent.
- The torque has to be calculated from the co-energy derivative method due to magnetic saturation.

- In general, the motor phases have almost zero interaction and thus SRM is claimed to be fault tolerant.
- The SRM is a motor totally dependent on the unipolar current two-quadrant multiphase chopper.
- One or, at most, two-phases may conduct at a time.
- Torque pulsations are reduced by torque sharing and current profiling, when a precision position sensor (estimator) is required.
- While low grade - general purpose - SRM drives are not difficult to control, high grade (servo) SRM drives require notable on-line (and off-line) computation efforts.
- The flux/current/position curve family is required for high grade (servo) SRM drives with motion sensors or sensorless.
- These curves are either FEM calculated or measured at standstill or in running (dynamic) tests. They are also curve fitted through analytical functions or mapped by a fuzzy logic approach.
- SRMs are simple and rugged, may withstand thermally harsh environments (like avionics, metalurgy, etc.) and thus, despite their more complicated control (for high grade performance), they seem to have a future. An incipient market has surfaced and strong marketing strides seem close.
- Single controlled power switch single phase SRM drives at low power seem feasible apparently for 4 quadrant operation in light start residential and automotive applications.

12.15. PROBLEMS

12.1. A 6/4 three-phase SRM has the data: maximum current i_{omax} = 10A, unaligned inductance L_u = 10mH, aligned inductance $L_a^s = 6L_u$; flux/current/position curves are considered piece-wise linear (Figure 12.22). The stator pole width angle β_s = 30°. The interpole width angle is β_i = 30°. The DC link voltage V_d = 300V for the unipolar current PWM converter.

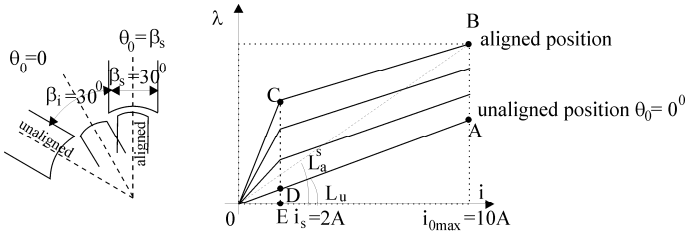

Figure 12.25. Linear piece-wise flux / current curve and unaligned and aligned position

Determine:

12.2. the maximum flux linkage;

12.3. the base speed ω_b for zero advance angle ($\theta_0 = 0°$);

12.4. the maximum average torque at zero speed;

12.5. torque versus position for constant current $i_{av} = 5A$;

12.6. for $\theta_c = -5°$ and $\theta_{off} = 22°$ calculate the maximum flux level in the phase at $2\omega_b$; determine the corresponding current from flux / current / position curves in Figure 12.22.

12.7. For the SRM of problem 12.1 and constant $\theta_{on} = \theta_0 = 0°$ and $\theta_{off} = 24°$ use Simulink to investigate the starting transients from zero to base speed with a load of 50% of maximum average torque at zero speed and the controller in example 12.5.

12.16. SELECTED REFERENCES

1. **T.J.E. Miller,** Switched reluctance motors and their control, OUP, 1993.
2. **C. Ferreira, E. Richter,** About channel independence for multichannel switching reluctance generating systems, Record of IEEE-IAS, Annual Meeting, 1996, pp.816-821.
3. **D.A. Philips,** Switched reluctance drive, new aspects, IEE Trans., vol.PE-5, no.4, 1990, pp.454-458.
4. **T.J.E. Miller,** Converter volt-ampere requirements of the switched reluctance motor drive, IEEE Trans., vol.IA-21, no.5, 1985, pp.1136-1144.
5. **W.F. Ray, P.L. Lawrenson et al.,** High performance switched reluctance brushless drives, IBID, vol.IA-22, no.4, 1986, pp.722-730.
6. **F. Liang, Y. Liao and T.A. Lipo,** A new variable reluctance motor utilizing an auxiliary commutation winding, IBID, 1993.
7. **H.Y. Li, Y.Zhao, T.A. Lipo and F. Liang,** A doubly salient doubly excited variable reluctance motor, Record of IEEE-IAS, Annual Meeting, 1992.
8. **B.C. Mecrow,** New winding configurations of doubly salient reluctance machines, Record of IEEE-IAS, Annual Meeting, 1992, Part.I, pp.249-256.
9. **P. Materu, R. Krishnan,** Estimation of switched reluctance motor losses, Record of IEEE-IAS, Annual Meeting, 1988, vol.I, pp.176-187.
10. **Y. Hayashi, T.J.E. Miller,** A new approach to calculating core losses in the SRM, IBID, 1994, vol.I, pp.322-328.
11. **V.V. Athani, V.N. Walivadeker,** Equivalent circuit for switched reluctance motor, EMPS vol.22, no.4, 1994, pp.533-543.
12. **I.A. Byrne, J.B. O'Dwyer,** Saturable variable reluctance machine simulation using exponential functions, Proc. of Int. Conf. on Stepping motors and systems, University of Leeds, July 1976, pp.11-16.
13. **D. Torrey**, An experimentally verified variable reluctance machine model implemented in the Saber ™ circuit simulation, EMPS Journal, vol.23, 1995.
14. **A. Cheok, N. Ertugrul**, A model-free fuzzy-logic-based rotor position sensorless switched reluctance motor drive, Record of IEEE-IAS, Annua1 Meeting, 1996, vol.I, pp.76-83.
15. **A. Radun**, Design considerations for the switched reluctance motor, Record of IEEE-IAS, Annual Meeting, 1994, vol.I, pp.290-297.
16. **B.K. Bose, T.J.E. Miller**, Microcomputer control of switched reluctance motor, Record of

IEEE-IAS, Annual Meeting, 1985, pp.542-547

17. **P.C. Kjaer, J.J. Gribble, T.J.E. Miller**, High grade control of switched reluctance machines, Record of IEEE-IAS, Annual Meeting, 1996, vol.I, pp.92-100.
18. **J.T. Buss, M. Eshani, T.J.E. Miller**, Robust torque control of SRM without a shaft-position sensor, IEEE Trans., vol.IA-33, no.3, 1996, pp.212-216.
19. **K. Rajashekara, A. Kawamura, K. Matsuse** (editors), Sensorless control of AC drives, IEEE Press, 1996, pp.433-485.
20. **P.P. Acarnley, C.D. French, IH. Al-Bahadly**, Position estimation in switched-reluctance drives, Record of EPE-95, Sevilla, Spain, pp.3765-3770.
21. **M.S. Islam, M.M. Anwar, I. Husain,** "A sensorless wide-speed range SRM drive with optimally designed critical rotor angles", Record of IEEE – IAS – 2000 Annual Meeting.
22. **R.B. Inderca, R.W. De Doncker,** "High dynamic direct torque control for switched reluctance drives", Record of IEEE – IAS – 2001 Annual Meeting.
23. **M. Eshani, B. Fahimi,** "Position sensorless control of switched reluctance motor drives", IEEE Trans. Vol. IE – 49, no. 1, 2002, pp.40-48.
24. **B. Fahimi, A Emadi, R.B. Sepe,** "Position sensorless control", IEEE – IAS Applications Magazine, vol. 10, 2004, pp. 40-47.
25. **R. Krishnan,** Switched reluctance motor drives, book, CRC Press, Florida, 2002.
26. **T. Higuchi, J.O. Fiedler, R.W. De Doncker,** "On the design of a single-phase switched reluctance motor", Record of IEEE – IEMDC – 2003, pp. 561-567.
27. **R. Krishnan, A.M. Staley, K. Sitapati,** "A novel single phase switched reluctance motor drive", Record of IEEE – IECON – 2001, pp. 1488-1493.
28. **R. Krishnan, S.T. Park, K. Ha,** "Theory and operation of a four quadrant SRM drive with a single controllable switch – the lowest cost four quadrant brushless motor drive", Record of IEEE –IAS – 2004 Annual Meeting.